





# High-mass MALDI-MS unravels ligand-mediated G protein-coupling selectivity to GPCRs

## Journal Article

### Author(s):

Wu, Na ; Olechwiec, Agnieszka M.; Brunner, Cyrill; Edwards, Patricia; Tsai, Ching-Ju ; Tate, Christopher G.; Schertler, Gebhard F.X.; Schneider, Gisbert ; Deupi, Xavier; Zenobi, Renato ; Ma, Pkyee

### Publication date:

2021-08-03

### Permanent link:

<https://doi.org/10.3929/ethz-b-000500012>

### Rights / license:

[Creative Commons Attribution 4.0 International](#)

### Originally published in:

Proceedings of the National Academy of Sciences of the United States of America 118(31), <https://doi.org/10.1073/pnas.2024146118>

### Funding acknowledgement:

160805 - Targeting Cancer Cells with Hybrid and Heterovalent Ligands at Controlled Distances (SNF)  
178765 - Soft ionization mass spectrometry for studying noncovalent interactions (SNF)

1  
2 **Main Manuscript for**

3  
4 **High-mass MALDI-MS unravels ligand-mediated G-protein coupling**  
5 **selectivity to GPCRs**

6  
7 Na Wu<sup>a</sup>, Agnieszka M. Olechwiec<sup>b,c</sup>, Cyrill Brunner<sup>a</sup>, Patricia C. Edwards<sup>d</sup>, Ching-Ju Tsai<sup>b</sup>,  
8 Christopher G. Tate<sup>d</sup>, Gebhard F.X. Schertler<sup>b,c</sup>, Gisbert Schneider<sup>a</sup>, Xavier Deupi<sup>b,e</sup>, Renato  
9 Zenobi<sup>a\*</sup>, Pikyee Ma<sup>b\*</sup>

10  
11 <sup>a</sup> Department of Chemistry and Applied Biosciences, ETH Zurich, CH-8093 Zurich, Switzerland.

12 <sup>b</sup> Laboratory of Biomolecular Research, Paul Scherrer Institute, CH-5232 Villigen PSI,  
13 Switzerland. <sup>c</sup> Department of Biology, ETH Zürich, CH-8093 Zürich, Switzerland. <sup>d</sup> Medical  
14 Research Council Laboratory of Molecular Biology, Francis Crick Avenue, Cambridge, CB2 0QH,  
15 UK. <sup>e</sup> Condensed Matter Theory Group, Paul Scherrer Institute, CH-5232 Villigen PSI,  
16 Switzerland.

17  
18 \*Correspondence to: Renato Zenobi (zenobi@org.chem.ethz.ch); Pikyee Ma (pik-ye.ma@psi.ch)

19  
20 **Author contributions:** N.W., R.Z., X.D. and P.M. designed the experiments. N.W. performed all  
21 the mass spectrometry experiments and all the related data processing. A.M.O. and P.M. produced  
22 and purified AT1R and  $\beta$ 1AR, C.-J.T. produced and purified rhodopsin. A.M.O., P.C.E., C.-J.T.  
23 and P.M. produced and purified mG $\alpha$ , heterotrimeric G proteins and Nb80. C.B. performed the  
24 microscale thermophoresis experiments and the related data processing. N.W., C.G.T., X.D.,  
25 G.F.X.S., G.S, R.Z. and P.M. interpreted the data. R.Z. and P.M. managed the overall project. The  
26 manuscript was written by N.W., X.D., R.Z. and P.M., and included contributions from all authors.

27  
28 **Competing Interest Statement:** G.F.X.S. declares that he is a cofounder and scientific advisor of  
29 the companies leadXpro AG and InterAx Biotech AG. C.G.T. is a shareholder, consultant and  
30 member of the scientific advisory board of Sosei Heptares. G.S. is a co-founder of inSili.com LLC  
31 and a consultant to the pharmaceutical industry.

32  
33 **Classification:** Biological Sciences – Biochemistry

34  
35 **Keywords:** G-protein-coupled receptors, high-mass MALDI mass spectrometry, protein-protein  
36 interactions, coupling selectivity, ligand screening method

37  
38 **This PDF file includes:**

39 Main Text

40 Figures 1 to 6

47 **ABSTRACT:**

48 G-protein-coupled receptors (GPCRs) are important pharmaceutical targets for the treatment of a  
49 broad spectrum of diseases. Although there are structures of GPCRs in their active conformation  
50 with bound ligands and G-proteins, the detailed molecular interplay between the receptors and  
51 their signaling partners remains challenging to decipher. To address this, we developed a high-  
52 sensitivity, high-throughput mass spectrometry method to interrogate the first stage of signal  
53 transduction. GPCR•G-protein complex formation is detected as a proxy for the effect of ligands  
54 on GPCR conformation and on coupling selectivity. Over 70 ligand•GPCR•partner protein  
55 combinations were studied using as little as 1.25 pmol protein per sample. We determined the  
56 selectivity profile and binding affinities of three GPCRs (rhodopsin, beta-1 adrenergic receptor  
57 [ $\beta$ 1AR], and angiotensin II type 1 receptor) to engineered  $G\alpha$  proteins (mGs, mGo, mGi, mGq)  
58 and nanobody 80. We found that GPCRs in the absence of ligand can bind mGo, and that the role  
59 of the G-protein C-terminus in GPCR recognition is receptor-specific. We exemplified our  
60 quantification method using  $\beta$ 1AR and demonstrated the allosteric effect of Nb80 binding in  
61 assisting displacement of nadolol to isoprenaline. We also quantify complex formation with wild-  
62 type heterotrimeric  $G\alpha_i\beta\gamma$  and  $\beta$ -arrestin 1 and showed that carvedilol induces an increase in  
63 coupling of  $\beta$ -arrestin 1 and  $G\alpha_i\beta\gamma$  to  $\beta$ 1AR. A normalization strategy allows us to quantitatively  
64 measure the binding affinities of GPCRs with partner proteins. We anticipate that this  
65 methodology will find broad use in screening and characterization of GPCR-targeting drugs.

66

67 **SIGNIFICANCE STATEMENT:**

68 G-protein-coupled receptors (GPCRs) are important pharmaceutical targets for the treatment of a  
69 broad spectrum of diseases. Upon ligand binding, GPCRs initiate intracellular signaling pathways  
70 by interacting with partner proteins. Assays that quantify the interplay between ligand binding and  
71 initiation of downstream signaling cascades are critical in the early stages of drug development.  
72 We have developed a high-throughput mass spectrometric method to unravel GPCR-protein  
73 complex interplay and demonstrated its use with three GPCRs to provide quantitative information  
74 about ligand-modulated coupling selectivity. This method provides new insights into the molecular  
75 details of GPCR interactions and could serve as a new approach for discovery of drugs that initiate  
76 specific cell signaling pathways.

77

78 **INTRODUCTION**

79 G-protein-coupled receptors (GPCRs) are the largest family of membrane receptors in  
80 humans and play essential roles in physiology and disease (1). Their physiological and cellular  
81 signaling effects, modulated by chemically diverse ligands, are exerted through coupling to and  
82 activating heterotrimeric G-protein complexes ( $G\alpha\beta\gamma$ ). In humans, there are 16  $G\alpha$  subunits that  
83 are classified into four families ( $G\alpha_s$ ,  $G\alpha_i/o$ ,  $G\alpha_{q/11}$  and  $G\alpha_{12/13}$ ). Each  $G\alpha$  subunit is involved in a  
84 specific signal transduction pathway (2). Although our understanding of GPCR signaling has been  
85 greatly enhanced by the remarkable progress in GPCR structural biology (3–6), much remains to  
86 be discovered to fully understand the molecular mechanisms of allostery and ligand-induced  
87 coupling selectivity (or functional selectivity) between GPCRs and their cytoplasmic transducers  
88 (G-proteins, but also kinases and arrestins) that lead to precise signal transduction cascades and  
89 biased signaling (7, 8).

90 Investigation of the interplay between GPCRs, ligands, and intracellular binding partners  
91 is challenging due to the complexity of their interactions. The functional outcome of GPCR activity  
92 depends on a still poorly understood network of protein interactions. To date, there are no high-  
93 throughput methods to study every G-protein and its ability to couple to a given receptor under a  
94 standard set of conditions. Many GPCR assays use radio-/fluorescent-labelled ligand binding or  
95 measurement of second messenger molecules. More recent methods involve cell-based biosensors,  
96 including dynamic mass redistribution (DMR) and cellular dielectric spectroscopy (CDS), that  
97 display an overall cellular response and translate GPCR signaling into distinct optical or  
98 impedance readouts respectively (9, 10). However, these assays do not provide a direct readout of  
99 G-protein coupling to GPCRs. Current biophysical methods that measure such protein interactions  
100 directly to provide information on selectivity and affinity – such as surface plasmon resonance

101 (SPR), fluorescence resonance energy transfer (FRET), isothermal titration calorimetry (ITC) and  
102 analytical ultracentrifugation (AUC) – only provide limited information on dynamic protein  
103 interactions and either are not suited for high-throughput screening or lack information on all  
104 interacting components. Bioluminescence resonance energy transfer (BRET) has been extensively  
105 used over the last two decades to study GPCR-protein interactions; however, BRET requires  
106 labeling of the proteins and, because their level of expression can vary considerably, quantification  
107 can be difficult. Native electrospray ionization mass spectrometry (nESI-MS) has been  
108 successfully applied to study G-protein complexes and membrane proteins (11). However, it is  
109 difficult to find buffer conditions that are compatible with both ESI-MS and functional membrane  
110 proteins.

111         Here, we developed a quantitative high-mass matrix-assisted laser desorption/ionization  
112 mass spectrometry (MALDI-MS) strategy that combines chemical crosslinking and quantification  
113 based on an internal standard to assay the interplay between receptors, ligands, and interacting  
114 proteins. Our versatile method enabled us to: (i) elucidate the selectivity profile of G-proteins to  
115 GPCR; (ii) dissect the molecular details of complex formation and probe the conformational  
116 regulation of GPCRs in an unprecedented way; (iii) determine the binding constant values and  
117 characterize ligand-ligand and protein-protein competitions. This method has a much higher  
118 tolerance to buffer, salts, detergents, or lipids than ESI-MS (12). Moreover, it does not require any  
119 immobilization or chemical labelling of the purified proteins that might alter their bioactivity and  
120 integrity of the complexes during detection. Our high-throughput method (384 sample spots per  
121 MALDI plate) is sensitive (the required amount per sample is only 1.25 pmol), rapid (one spectrum  
122 can be recorded within 8 seconds), and quantitative. More than 70 ligand-GPCR-partner  
123 combinations were studied.

124

## 125 RESULTS

126 **Optimization of Crosslinking Reaction and Spotting Method.** The combination of crosslinking  
127 and mass spectrometry is a rapidly emerging approach to provide information on the structure and  
128 interaction networks of proteins (13, 14). The GPCR-G protein interaction is transient and the  
129 complex is considered to be intrinsically unstable (15). Thus, capturing this interaction requires  
130 the use of certain stratagems such as stabilization of the complexes with nanobodies or antibodies,  
131 or recombinant technology to prevent their dissociation.

132 Lysine residues are present at the G-protein interacting interfaces of GPCRs (*SI Appendix*,  
133 Fig. S1). Based on this, we used BS(PEG)<sub>9</sub>, a bifunctional amine reactive reagent with a spacer  
134 arm length of 38.5 Å (*SI Appendix*, Fig. S1), to crosslink interacting proteins via lysine residues.  
135 After reaction, samples will contain intramolecular crosslinks, monolinks, and, most importantly,  
136 intermolecular crosslinks (Fig. 1A) that stabilize and capture the protein-protein complexes in their  
137 equilibrium state, preventing them from dissociating during the MALDI process. We optimized  
138 experimental conditions and crosslinking times using the prototypical photoreceptor rhodopsin  
139 (Rho), which couples effectively to mGo (a truncated form of Gα<sub>o</sub> subunit) (16) (*SI Appendix*, Fig.  
140 S2). We found that even short (≤1 min) pre-incubation with BS(PEG)<sub>9</sub> prevents the association  
141 between Rho and mGo (*SI Appendix* Fig. S3), probably due to quick reaction of the crosslinker  
142 with lysine residues near the binding interfaces of Rho and mGo, precluding assembly of the  
143 complex. Using an optimized experimental procedure, we estimated that in all of the Gα proteins  
144 or their truncated versions tested, 6-9 lysine residues react with BS(PEG)<sub>9</sub> (*SI Appendix*, Table  
145 S1), resulting in the formation of ~2 intermolecular crosslinks in each complex (*SI Appendix*, Table  
146 S2).

147 GPCRs are extremely challenging integral membrane proteins to work with as they are  
148 unstable in detergent solution and require the use of an appropriate condition for their extraction  
149 from the membranes. Since they are available in low quantity only, a sensitive detection method  
150 will therefore help reduce protein sample consumption. Thus, we optimized the MALDI sandwich  
151 spotting method by trial and error by testing various chemicals and the number of layers in the  
152 sandwiching method, and found that addition of a third layer of saturated sinapinic acid  
153 considerably improved the signal level of GPCR proteins by MALDI detection and thus improved  
154 sensitivity (*SI Materials and Methods*). With this sensitivity, we were able to even detect picomole  
155 quantities of protein.

156  
157 **Ligand-Mediated GPCR Selective Coupling.** Using our optimized crosslinking protocol, we  
158 first showcase our method by examining the coupling ability of three class A GPCRs to a panel of  
159 mini-G $\alpha$  proteins (17) (hereafter abbreviated as mG $\alpha$ : mGs, mGo, mGi, mGq) and nanobody 80  
160 (Nb80) (18), in the presence or absence of various ligands (Fig. 2 and *SI Appendix* Table S3). The  
161 GPCRs studied were a constitutively active mutant of bovine Rho, thermostabilized turkey  $\beta$ 1AR,  
162 and the F117W mutant of mouse angiotensin II type 1 receptor (AT1R) (protein sequences: see  
163 Table S4).

164 Detection and analysis of multi-component proteins complexes (such as GPCRs with their  
165 heterotrimeric G proteins) by any biophysical method is challenging. We therefore established our  
166 method by using mG $\alpha$  proteins, which are simplified versions of their full-length counterpart (G $\alpha$ )  
167 containing the GTPase domain but lacking the  $\alpha$ -helical domain, and are widely used in  
168 biochemical, biophysical, cellular and structural biology studies for studying GPCR•G-protein  
169 interactions and GPCR activation mechanisms (6, 11, 19, 20). Swapping the c-tail ( $\alpha$ 5 helix) of the

170 G protein is commonly performed to switch selectivity between G-protein subtypes (21). Our mGo  
171 and mGs are thermostabilised version of their truncated wild-type G-protein, and mGq and mGi  
172 are engineered from mGs by introducing nine and seven mutations on the  $\alpha 5$  helix that correspond  
173 to residues of Gq and Gi, respectively (17). Mixing and incubation of the binding partners is  
174 followed by treatment with BS(PEG)<sub>9</sub>, and the resulting complexes and remaining unbound  
175 partners in the sample are detected by high-mass MALDI-MS by monitoring the peak intensities  
176 of each species. Examples of measured spectra are shown in Fig. 1B, the results are summarized  
177 in Fig. 2, and the full data set for all combinations is shown in *SI Appendix*, Fig. S4. Our method  
178 allows us to indirectly detect conformational changes and ensembles of the receptor by following  
179 receptor-complex formation, which can be read out directly from the mass spectra.

180 GPCR orthosteric ligands fall into three categories: activating (agonists), inactivating  
181 (inverse agonists) and neutral (antagonists). Our assay largely displays the expected GPCR•G-  
182 protein recognition patterns. The constitutively active Rho mutant couples to the two members of  
183 the  $G\alpha_{i/o}$  family, mGo and mGi, both in the apo (apo-Rho) and agonist-bound (atr-Rho) forms (Fig.  
184 2). This was expected, as constitutively active Rho has been shown to strongly recruit Gi and Go  
185 (16, 23, 24). The iso- $\beta 1$ AR was found to bind to Nb80 (a Gs mimetic nanobody), proving that our  
186  $\beta 1$ AR construct can achieve a fully active conformation and that Nb80 binding is conformation  
187 specific (25). It has been shown that this receptor can couple to  $G\alpha_s$ ,  $G\alpha_i$  and  $G\alpha_q$  families (26) and,  
188 indeed, we observe that agonist-bound  $\beta 1$ AR (iso- $\beta 1$ AR) can couple to some extent to all mG $\alpha$   
189 subtypes (Fig. 2). Apo- $\beta 1$ AR can specifically couple to mGo, which showed similar selectivity  
190 profiles with known antagonists (propranolol, nadolol, and carvedilol) and s32212. Based on these  
191 profiles, we can classify s32212 as an antagonist for  $\beta 1$ AR. Finally, we observed that our agonist-  
192 bound AT1R (angII-AT1R) couples to both mGq and mGo, but not mGi (Fig. 2). This could be



193 because our mGi construct lacks some key residues required for receptor binding (17). As mGi is  
194 engineered from mGs and contains only the Gi fragment on the  $\alpha 5$  helix, this suggests the  $\alpha 5$  helix  
195 of Gi is not the main determinant for its coupling to AT1R and instead the globular part of Gi could  
196 be more important. This may also explain why we observe a weak interaction of mGi to iso- $\beta 1$ AR  
197 and potentially weak interactions also to car- $\beta 1$ AR and angII-AT1R (Fig. 2). Azilsartan, a potent  
198 inverse agonist can compete off many AT1R blockers (22). We expect that this ligand stabilizes  
199 the receptor in an inactive conformation with severely impaired mG $\alpha$  coupling. Indeed, this ligand  
200 abolished coupling of all mG $\alpha$  proteins to the AT1R, including mGo (Fig. 2). These data illustrate  
201 how the apo, agonist-bound, antagonist-bound and inverse agonist-bound forms of receptors exist  
202 in different conformational ensembles with different profiles of G-protein recognition.

203 From the perspective of the mG $\alpha$  proteins, mGo is found to be the most promiscuous G-  
204 protein, as it binds to all agonist/antagonist-bound receptors and, remarkably, to all apo receptors  
205 (Fig. 2 and *SI Appendix*, Fig. S4). Native Go protein is highly expressed in the central and  
206 peripheral nervous systems, endocrine cells, and cardiomyocytes, being the most abundant G-  
207 protein subtype in neurons (27, 28). There is considerable evidence for the existence of functional  
208 complexes of apo-GPCRs with G-protein (29–33) and the Go subtype seems particularly  
209 predisposed to such pre-coupling (34, 35). Thus, we conjecture that the promiscuity of mGo  
210 observed in our assay represents its ability to recognize apo (through pre-coupling), agonist-bound  
211 and antagonist-bound receptors.

212

213 **A normalization strategy to determine binding Affinity of GPCR•partner Complexes.** Since  
214 ionisation efficiencies of proteins are highly variable in MALDI and could change upon  
215 crosslinking, there is no direct correlation between peak intensity and protein concentration. To be

216 able to quantify individual protein components in the spectra, we developed a normalization  
217 strategy using  $\beta$ -galactosidase ( $\beta$ -gal) as a reference protein (an example of calibration and  
218 standard curve for Rho is shown in Fig. 3A and B, and the rest of the data in *SI Appendix*, Fig. S5),  
219 which is stable in its monomeric form (*SI Appendix*, Fig. S6) and does not interfere with the  
220 analytes of the sample (*SI Appendix*, Fig. S7 and S8). This allowed us to calculate the  
221 concentrations of each species at equilibrium (*SI Appendix*, Fig. S9-S11) and the corresponding  
222 dissociation constants of the complexes between GPCRs and their partner proteins (Fig. 3C).

223         The measured dissociation constants between GPCRs and interacting proteins ( $K_d$ ) are in  
224 the high nanomolar to low micromolar range (summarized in Fig. 3 and *SI Appendix*, Table S5).  
225 Literature  $K_d$  values are scarce because such measurements are challenging. A comparison of the  
226 MALDI-based  $K_d$  data with literature and a microscale thermophoresis measurement showed good  
227 agreement (*SI Appendix*, Fig. S12, Table S6). We observed that mGo generally had a higher  
228 affinity to the GPCRs compared to other partner proteins (Fig. 3). For  $\beta$ 1AR, the dissociation  
229 constant of mGo (0.25  $\mu$ M) was hardly influenced by the ligands (Fig. 2 and *SI Appendix*, Fig. S4)  
230 and was considerably lower than that of mGs (0.35  $\mu$ M), mGq (1.24  $\mu$ M), and mGi (1.62  $\mu$ M).  
231 Among the receptors,  $\beta$ 1AR generally has higher affinities to the test partner proteins. For AT1R,  
232 binding to mGo is twice as strong than to mGq (Fig. 3, *SI Appendix*, Fig. S4 and Table S5). We  
233 quantitatively elucidated the interaction strength between the protein-protein complexes. These  
234 interactions are the key determinant of information transmission within a signaling network.

235  
236 **Effect of the G-protein C-terminus on the Interaction with GPCRs.** Many aspects of the  
237 formation of signaling complexes between GPCRs and G-proteins are still unclear, such as the  
238 molecular determinants of coupling selectivity (8) or the role of pre-coupling of G-proteins to

239 inactive receptors (34). Recent structural and biophysical studies have confirmed the C-terminus  
240 of the G $\alpha$  subunit as one of the primary determinants of the interaction with GPCRs (36, 37). The  
241 binding characteristics of our mG $\alpha$  constructs show indeed that a few amino acid substitutions in  
242 the C-terminus of mGs, mGi, and mGq can alter their selective coupling to AT1R and Rho and  
243 impact the binding affinity to  $\beta$ 1AR (Fig. 3). To further assess the role of the mG $\alpha$  C-terminus, we  
244 truncated the last five residues from mGo and mGi (mGo\_ $\Delta$ 5 and mGi\_ $\Delta$ 5) and assessed their  
245 binding affinity to our panel of receptors. Our data show that mGi truncation abolished coupling  
246 to both apo and agonist-bound receptors (Fig. 4 and *SI Appendix*, Fig. S13). However, truncation  
247 of mGo affected coupling to Rho and AT1R, but not to  $\beta$ 1AR, which still binds mGo\_ $\Delta$ 5 with  
248 similar affinities to mGo in both the apo (0.28  $\mu$ M) and agonist-bound (0.23  $\mu$ M) states. This  
249 indicates that the last five residues of G-protein are not always the main determinant for receptor  
250 recognition and other regions can mediate high-affinity binding (15, 21). Based on the observation  
251 that ligands did not affect the affinity between  $\beta$ 1AR and mGo, but had a significant effect on the  
252 binding of Rho and AT1R to mGo, we speculate that ligand-induced GPCR conformational  
253 changes have a greater influence on the C-terminal contribution of the binding to the G-protein,  
254 and that GPCR and mGo interactions are receptor-dependent.

255

256 **Ligand-Mediated Competition between Partner Proteins.** To explore the interplay between  
257 affinity and selectivity in GPCR binding partners, we measured the formation of  $\beta$ 1AR complexes  
258 with mG $\alpha$  proteins (mGs, mGo, and mGq) in the presence of the competitor Nb80 at equimolar  
259 amounts (Fig. 5A and *SI Appendix*, Fig. S14 A, B). In the absence of ligand,  $\beta$ 1AR binds only to  
260 mGo due to its pre-coupling ability (K<sub>d</sub> of 0.25 $\mu$ M) (Fig. 3), indicating that the ligand-free receptor  
261 ensemble is conformationally specific for mGo only. Isoprenaline-bound  $\beta$ 1AR selectively

262 coupled with Nb80 in the presence of mGs or mGq, but couple with both mGo and Nb80. This is  
263 due to the tighter binding of Nb80 for isoprenaline-bound  $\beta$ 1AR (0.21 $\mu$ M) compared to mGs (0.35  
264  $\mu$ M) and mGq (1.24  $\mu$ M), while mGo binds with similar affinity to Nb80 (0.25  $\mu$ M) (Fig. 3).

265 To measure the inhibition ability of Nb80 to mGo, we measured the formation of  
266  $\beta$ 1AR•mGo complexes at increasing concentrations of Nb80 (Fig. 5D and *SI Appendix*, Fig.  
267 S14C), and calculated the inhibitory constant ( $K_i$ ) of Nb80 to mGo (1.57 $\pm$ 0.24  $\mu$ M) (*SI Appendix*.  
268 Fig. S14 D and E). We also measured the effects of isoprenaline on the competition between mGo  
269 and Nb80, and as expected, the competitiveness of Nb80 increases with rising isoprenaline  
270 concentration (*SI Appendix*, Fig. S15). These results show that when multiple partner proteins  
271 coexist, while GPCRs prefer to couple with partners of higher affinity, changes in ligand and  
272 partner concentrations can alter this coupling selectivity. We can substantiate that the promiscuous  
273 binding of mGo is specific for the two following reasons: first, we were able to displace mGo  
274 binding to AT1R in the present of the inverse agonist azilsartan, showing that mGo binding can be  
275 allosterically modulated by ligands (Fig. 2B). Second, Nb80 can also displace mGo binding to  
276  $\beta$ 1AR in a competitive manner (Fig. 5D). These results strongly suggest that mGo binds to the  
277 ‘canonical’ recognition site in the cytoplasmic side of the activated receptor.

278

279 **Allosteric Influence of Ligands on GPCRs.** We also investigated the allosteric conformational  
280 regulation of GPCR•G-protein complexes by several ligands (Fig. 5B, C and *SI Appendix*, Fig.  
281 S16). All antagonists tested had the same effect on the coupling ability of  $\beta$ 1AR, which binds only  
282 to mGo in their presence (Fig. 2). To further characterize these antagonists, we measured their  
283 ability to compete with the agonist and affect formation of the receptor•mG $\alpha$  complexes by  
284 incubating 2.5  $\mu$ M apo- $\beta$ 1AR with equimolar amounts (50  $\mu$ M) of antagonist (s32212,

285 propranolol, carvedilol or nadolol) and agonist (isoprenaline) (Fig. 5B and C, and *SI Appendix*,  
286 Fig. S16). At these concentrations, isoprenaline cannot compete off propranolol or carvedilol, and  
287 propranolol/carvedilol-bound  $\beta$ 1AR still only recruits mGo, but it can compete off s32212 and  
288 recovers coupling to mGs, Nb80, and, partially, to mGq. Interestingly, in nadolol-bound  $\beta$ 1AR,  
289 isoprenaline only partially recovers its recruiting ability with Nb80, but not with mGs and mGq  
290 (*SI Appendix*, Fig. S16).

291 We next explored in more detail the inhibitory ability of these antagonists on the formation  
292 of GPCR complexes. For that, we measured the formation of the  $\beta$ 1AR•mGs and  $\beta$ 1AR•Nb80  
293 complexes in the presence of 1 or 25  $\mu$ M of antagonists at increasing concentrations of isoprenaline  
294 (Fig. 5E and F, and *SI Appendix*, Fig. S17). S32212 behaves as a surmountable competitive  
295 antagonist, as raising the isoprenaline concentration recovers near-maximal formation of the  
296  $\beta$ 1AR•mGs complex (80%); the  $K_i$  of s32212 was determined to be  $3.56 \pm 0.26 \mu$ M (*SI Appendix*,  
297 Fig. S17 and S18). On the contrary, propranolol behaves as an insurmountable competitive  
298 antagonist, as isoprenaline (at any concentration) cannot recover maximal  $\beta$ 1AR•mGs complex  
299 formation. Nadolol shows dual behaviour in different complex systems: it is insurmountable in  
300  $\beta$ 1AR•mGs but surmountable in  $\beta$ 1AR•Nb80 (Fig. 5F), likely due to the higher affinity of Nb80  
301 with isoprenaline-bound  $\beta$ 1AR compared to mGs, and the allosteric effect of Nb80, which assists  
302 displacement of nadolol to isoprenaline. The positive cooperative effect of Nb80 on isoprenaline  
303 binding we observe here is consistent with a previous report (38) and demonstrates the allosteric  
304 mechanistic property of GPCRs. Our data agree with the concept that ligands induce (or stabilize)  
305 specific receptor conformations and the sensitivity of our method reveals in detail the complexity  
306 of their interactions. We showed that nadolol is more surmountable than propranolol, in agreement  
307 with their reported  $pK_i$  values (-8.2 and -7.2, respectively) (*SI Appendix*, Table S3). Furthermore,

308 we show for the first time that S32212 is a weaker antagonist for  $\beta$ 1AR than nadolol, as shown by  
309 its less prominent inhibitory effect (Fig. S16).

310  
311 **Ligand-Biased Assembly of the  $\beta$ 1AR•G Protein/Arrestin Complexes.** Next, we expanded our  
312 method by using full-length wild-type protein partners –  $G\alpha_i\beta\gamma$  and  $\beta$ -arrestin-1 (Fig. 6). We first  
313 incubated apo-, isoprenaline-, or carvedilol-bound  $\beta$ 1AR with  $G\alpha_i$ ,  $G\alpha_i\cdot G\beta\cdot G\gamma$  or  $\beta$ -arrestin-1 at  
314 equimolar concentration and tested the formation of  $\beta$ 1AR•protein complexes. Artefacts were  
315 excluded by measuring mixtures of proteins that were pre-treated with the crosslinker, which could  
316 not form protein complexes (Fig. 6B). We found that isoprenaline-bound  $\beta$ 1AR and ligand-free  
317  $\beta$ 1AR exhibited similar binding affinity to  $G\alpha_i$  and arrestin (~60% and 32% complex formation,  
318 respectively), while carvedilol-bound  $\beta$ 1AR showed a higher affinity to  $G\alpha_i$  and arrestin (~92%  
319 and 88% complex formation, respectively). We also tested the complex formation in an equimolar  
320 mixture of  $\beta$ 1AR,  $G\alpha_i$ , and arrestin. We found that both the  $\beta$ 1AR• $G\alpha_i$  and  $\beta$ 1AR•arrestin  
321 complexes were present, but that the former formed much more readily than the latter (four times  
322 higher intensity with apo- or iso- $\beta$ 1AR and three times higher intensity with car- $\beta$ 1AR). This also  
323 illustrates that  $G\alpha_i$  possesses a higher binding affinity with  $\beta$ 1AR than arrestin.

324 We then studied the interaction between ligand-bound  $\beta$ 1AR and  $G\alpha_i\cdot G\beta\cdot G\gamma$ . We  
325 incubated  $G\alpha_i$  with  $G\beta\cdot G\gamma$  at equimolar concentration, and, as expected, we detected peaks for the  
326 crosslinked complexes  $G\beta\cdot G\gamma$  (47,600 Da) and  $G\alpha_i\cdot G\beta\cdot G\gamma$  (91,500 Da) (Fig. 6C). Additionally,  
327 we observed a peak  $m/z$  at 53,200 Da corresponding to a cross-linked complex of  $G\alpha_i$  with  $G\gamma$   
328 (Fig. 6C and *SI Appendix*, Fig. S19). Following addition of  $\beta$ 1AR, we observed the simultaneous  
329 presence of the cross-linked complexes  $G\alpha_i\cdot G\gamma$ ,  $G\alpha_i\cdot G\beta\cdot G\gamma$ ,  $\beta$ 1AR• $G\alpha_i$  (82,800 Da) and  
330  $\beta$ 1AR• $G\alpha_i\cdot G\beta\cdot G\gamma$  (130,900 Da) (Fig. 6C). The presence of isoprenaline hardly altered the relative

331 intensity of these protein peaks compared to the absence of ligand, while carvedilol increased the  
332 formation of  $\beta 1AR \cdot G\alpha_i \cdot G\beta \cdot G\gamma$  resulting in a complete disappearance of the  $\beta 1AR$ ,  $G\beta \cdot G\gamma$ , and  
333  $G\alpha_i \cdot G\gamma$  peaks. As car- $\beta 1AR$  does not bind mGi (Fig. 2), these data show that mGi did not inherit  
334 all the bioactivity from Gi, indicating that other regions of the  $G\alpha$  core domain make a large  
335 contribution to its receptor binding specificity. Our receptors were not treated with kinases or  
336 phosphorylation enzymes; in addition, our  $\beta 1AR$  construct is truncated at the C-terminus and  
337 intracellular loop 3, meaning that the majority of the phosphorylation sites are absent. The absence  
338 of phosphorylation, which precludes PKA-dependent Gs/Gi switching in the  $\beta 1AR$  (39), is the  
339 probable cause of the lack of  $G\alpha_i \cdot G\beta \cdot G\gamma$  recruitment observed for iso- $\beta 1AR$  (i.e., same response  
340 than the apo receptor; Fig. 6C). Moreover, our data suggest that carvedilol-mediated arrestin  
341 coupling to  $\beta 1AR$  is phosphorylation-independent. Importantly, our method allows the  
342 quantification of Gi- and arrestin-complex formation induced by carvedilol, which quantitatively  
343 shows how ligands modulate the extent of the recruitment of G-proteins and arrestin.

344

## 345 **DISCUSSION**

346 Several recent technological advances have enhanced our understanding of various aspects of  
347 GPCR activation mechanisms and signaling. For example, structural biology studies by NMR, X-  
348 ray crystallography and cryo-EM have provided high-resolution structural insights, enabling the  
349 molecular characterization of different protein complexes. In addition, functional studies using  
350 biophysical and signaling assays have allowed the characterization of ligand properties and ligand-  
351 mediated cellular response. However, the characterization of the network of GPCR-protein  
352 interactions following receptor activation remains difficult to tackle. While the traditional view of  
353 GPCR signaling involves a more or less sequential course of events, it is now clear that receptors

354 can adopt multiple active states and engage multiple intracellular binding partners in a complex  
355 interaction network. To better understand the network of ligand-mediated GPCR•G-protein  
356 interactions, we developed a method to address this by directly monitoring the GPCR-protein  
357 complex formation. We demonstrated the use of our method by screening three class A GPCRs  
358 against a panel of engineered G $\alpha$  proteins and generated a selectivity profile for each ligand tested  
359 (Fig. 2B). In agreement with a previous study (21), a G $_{i/o}$ -coupled receptor (Rho in this case) is  
360 more selective and couples only to G $_i$  and G $_o$ . Our G $_s$ - and G $_q$ -coupled receptors ( $\beta$ 1AR and AT1R)  
361 are more promiscuous and always couple to some extent to the G $_{i/o}$  family as well (Fig. 2B). In  
362 order to fully understand the promiscuity of agonist-bound receptors, probably high-resolution  
363 structures of the same receptor bound to different transducers would be required to provide the  
364 molecular details and insights into this aspect.

365         The selectivity profiles of our three GPCRs indicate that each ligand-free or ligand-bound  
366 receptor has its unique coupling profile (Fig. 2B). Concurring with previous studies, we also show  
367 that agonist-bound GPCRs exist in multiple conformations (Fig. 2). This explains the complexity  
368 of the GPCR signaling mechanism, which is not governed simply by ‘active’ and ‘inactive’ states,  
369 or a ternary model. The method presented here allows us to investigate GPCR interactions in an  
370 unprecedented way. The proportion of different ligands (agonist and antagonist) can further fine-  
371 tune the receptor conformational ensembles (Fig. S16). Thus, our data enable us to observe the  
372 allosteric conformational regulation of GPCRs, which helps to explicate the plasticity of GPCR  
373 signal transduction.

374         The development and application of efficient GPCR binding assays are critical in the early  
375 stages of drug development. Current high-throughput technologies for assaying the function of  
376 GPCRs mainly depend on the measurement of second messenger output, such as inositol



377 phosphate, calcium and cAMP. These readouts are distant from the actual information of the  
378 GPCR-effector complex, and rely on cellular responses that can be modulated by several separate  
379 or even cross-talking signaling pathways. Therefore, the second messenger output does not directly  
380 indicate the ‘recruiting’ activity of a ligand and does not provide an accurate way to profile ligands  
381 according to this measure. Unraveling the relationships between ligand, receptor, and the coupling  
382 complexes (with G proteins and arrestins) that mediate downstream signaling events is the key to  
383 unscramble allostereism and biased signaling. We showed that our method can effectively be used  
384 to study the coupling of both G protein and arrestin (Fig. 6) and thus could potentially be used in  
385 drug discovery for ligand profiling.

386 Investigating the pentameric complex system (ligand• $\beta$ 1AR•G $\alpha_i$ •G $\beta$ •G $\gamma$ ) (Fig. 6C) was  
387 more complicated than the three-component systems (ligand•GPCR•mG $\alpha$ /G-protein/arrestin) and  
388 posed a challenge to obtain the binding affinity values for all components. However, our data  
389 provide a unique profile for such pentameric system at equilibrium (Fig. 6C). Further expansion  
390 of our method to study other members of the G protein, arrestin and G-protein kinase families may  
391 be of great relevance to future GPCR deorphanization approaches, or to dissect partially  
392 overlapping signaling pathways occurring in some of the G protein families, such as the Gi/o/z.

393 GPCRs are allosterically dynamic proteins. Multiple biophysical techniques are currently  
394 being used to fully understand how different ligands produce different signaling patterns.  
395 Complementary to previous techniques, our strategy represents the first mass spectroscopic  
396 method that allows characterization of the direct ligand-induced receptor-protein complex  
397 formation in detail. We developed a powerful all-in-one method, unraveling the G-protein  
398 coupling selectivity to GPCRs and receptor conformational regulation, to provide information  
399 regarding the protein/analyte concentrations, their competition, affinity constants, molecular size

400 and structure. We therefore anticipate that our method will emerge as a valuable strategy for high-  
401 throughput screening and for unravelling the molecular details of ligand-GPCR-protein  
402 interaction.

403

## 404 **MATERIALS AND METHODS**

405 Detailed materials and methods are provided in *SI Materials and Methods*. This includes detailed  
406 information about materials used, methodology and experiment protocols, mass spectra and data  
407 analysis, MST data, three-dimensional models of the tested proteins, tables of the number of  
408 intermolecular crosslinks present in each complex, information of ligands, and amino acid  
409 sequences of the proteins.

410

## 411 **ACKNOWLEDGEMENTS**

412 We are grateful to Chundong Ni and Przemyslaw Nogly for helpful discussions. We thank  
413 Matthew Rodrigues and Volodymyr Korkhov for their careful reading of our paper. We thank  
414 Jonas Mühle for the arrestin protein, Filip Pamula for helping with G $\alpha$ i purification, Daniel Mayer  
415 for the  $\beta$ 1AR construct, and to H.G. Khorana for providing HEK293 GntI-cells. We acknowledge  
416 the Swiss National Science Foundation for grants 310030B\_173335 (to G.F.X.S), CRSII2\_160805  
417 and 310030\_192780 (to X.D.), and 200020\_178765 (to R.Z.); Support from the Chinese  
418 Scholarship Council (to NW, project # 201709370040) and from the Holcim Stiftung (to PM) is  
419 gratefully acknowledged.

420

421

422

423 **DATA AND MATERIALS AVAILABILITY**

424 The original data used in this publication are made available in a curated data archive at ETH  
425 Zurich (<https://www.researchcollection.ethz.ch>) under the DOI 10.3929/ethz-b-000482980.

426

427 **REFERENCES**

428

- 429 1. A. S. Hauser, M. M. Attwood, M. Rask-Andersen, H. B. Schiöth, D. E. Gloriam, Trends in GPCR drug  
430 discovery: new agents, targets and indications. *Nat Rev Drug Discov* **16**, 829–842 (2017).
- 431 2. G. Milligan, E. Kostenis, Heterotrimeric G-proteins: a short history. *Br. J. Pharmacol.* **147 Suppl 1**, S46-55  
432 (2006).
- 433 3. D. Hilger, M. Masureel, B. K. Kobilka, Structure and dynamics of GPCR signaling complexes. *Nat. Struct.*  
434 *Mol. Biol.* **25**, 4–12 (2018).
- 435 4. X. E. Zhou, K. Melcher, H. E. Xu, Understanding the GPCR biased signaling through G protein and arrestin  
436 complex structures. *Curr. Opin. Struct. Biol.* **45**, 150–159 (2017).
- 437 5. A. Inoue, *et al.*, Illuminating G-Protein-Coupling Selectivity of GPCRs. *Cell* **177**, 1933-1947.e25 (2019).
- 438 6. J. García-Nafria, C. G. Tate, Cryo-EM structures of GPCRs coupled to Gs, Gi and Go. *Mol. Cell. Endocrinol.*  
439 **488**, 1–13 (2019).
- 440 7. J. W. Wisler, K. Xiao, A. R. B. Thomsen, R. J. Lefkowitz, Recent developments in biased agonism. *Curr.*  
441 *Opin. Cell Biol.* **27**, 18–24 (2014).
- 442 8. A. Glukhova, *et al.*, Rules of Engagement: GPCRs and G Proteins. *ACS Pharmacol Transl Sci* **1**, 73–83  
443 (2018).
- 444 9. R. Schröder, *et al.*, Deconvolution of complex G protein-coupled receptor signaling in live cells using  
445 dynamic mass redistribution measurements. *Nat. Biotechnol.* **28**, 943–949 (2010).
- 446 10. K. Miyano, *et al.*, History of the G protein-coupled receptor (GPCR) assays from traditional to a state-of-the-  
447 art biosensor assay. *J. Pharmacol. Sci.* **126**, 302–309 (2014).
- 448 11. H.-Y. Yen, *et al.*, PtdIns(4,5)P2 stabilizes active states of GPCRs and enhances selectivity of G-protein  
449 coupling. *Nature* **559**, 423–427 (2018).
- 450 12. F. Chen, *et al.*, High-Mass Matrix-Assisted Laser Desorption Ionization-Mass Spectrometry of Integral  
451 Membrane Proteins and Their Complexes. *Anal. Chem.* **85**, 3483–3488 (2013).
- 452 13. L. Piersimoni, A. Sinz, Cross-linking/mass spectrometry at the crossroads. *Anal Bioanal Chem* **412**, 5981–  
453 5987 (2020).
- 454 14. C. Iacobucci, M. Götze, A. Sinz, Cross-linking/mass spectrometry to get a closer view on protein interaction  
455 networks. *Curr. Opin. Biotechnol.* **63**, 48–53 (2020).

- 456 15. Y. Du, *et al.*, Assembly of a GPCR-G Protein Complex. *Cell* **177**, 1232-1242.e11 (2019).
- 457 16. C.-J. Tsai, *et al.*, Crystal structure of rhodopsin in complex with a mini-G<sub>s</sub> sheds light on the principles of G  
458 protein selectivity. *Science Advances* **4**, eaat7052 (2018).
- 459 17. R. Nehmé, *et al.*, Mini-G proteins: Novel tools for studying GPCRs in their active conformation. *PLoS ONE*  
460 **12**, e0175642 (2017).
- 461 18. A. Manglik, B. K. Kobilka, J. Steyaert, Nanobodies to Study G Protein-Coupled Receptor Structure and  
462 Function. *Annu. Rev. Pharmacol. Toxicol.* **57**, 19–37 (2017).
- 463 19. Q. Wan, *et al.*, Mini G protein probes for active G protein-coupled receptors (GPCRs) in live cells. *J Biol*  
464 *Chem* **293**, 7466–7473 (2018).
- 465 20. B. Carpenter, C. G. Tate, Engineering a minimal G protein to facilitate crystallisation of G protein-coupled  
466 receptors in their active conformation. *Protein Eng. Des. Sel.* **29**, 583–594 (2016).
- 467 21. N. Okashah, *et al.*, Variable G protein determinants of GPCR coupling selectivity. *PNAS* **116**, 12054–12059  
468 (2019).
- 469 22. M. Ojima, *et al.*, In vitro antagonistic properties of a new angiotensin type 1 receptor blocker, azilsartan, in  
470 receptor binding and function studies. *J Pharmacol Exp Ther* **336**, 801-808 (2011).
- 471 23. X. Deupi, *et al.*, Stabilized G protein binding site in the structure of constitutively active metarhodopsin-II.  
472 *Proc. Natl. Acad. Sci. U.S.A.* **109**, 119–124 (2012).
- 473 24. C.-J. Tsai, *et al.*, Cryo-EM structure of the rhodopsin-G<sub>ai</sub>- $\beta\gamma$  complex reveals binding of the rhodopsin C-  
474 terminal tail to the  $\beta\gamma$  subunit. *Elife* **8** (2019).
- 475 25. S. Isogai, *et al.*, Backbone NMR reveals allosteric signal transduction networks in the  $\beta_1$ -adrenergic receptor.  
476 *Nature* **530**, 237–241 (2016).
- 477 26. F. Li, M. D. Godoy, S. Rattan, Role of Adenylate and Guanylate Cyclases in  $\beta_1$ -,  $\beta_2$ -, and  $\beta_3$ -Adrenoceptor-  
478 Mediated Relaxation of Internal Anal Sphincter Smooth Muscle. *J Pharmacol Exp Ther* **308**, 1111–1120  
479 (2004).
- 480 27. C. W. Luetje, K. M. Tietje, J. L. Christian, N. M. Nathanson, Differential tissue expression and developmental  
481 regulation of guanine nucleotide binding regulatory proteins and their messenger RNAs in rat heart. *J. Biol.*  
482 *Chem.* **263**, 13357–13365 (1988).
- 483 28. M. Jiang, N. S. Bajpayee, Molecular mechanisms of go signaling. *Neurosignals* **17**, 23–41 (2009).
- 484 29. M. Yanagawa, *et al.*, Single-molecule diffusion-based estimation of ligand effects on G protein-coupled  
485 receptors. *Sci Signal* **11** (2018).
- 486 30. G. Navarro, *et al.*, Evidence for functional pre-coupled complexes of receptor heteromers and adenylyl  
487 cyclase. *Nat Commun* **9**, 1242 (2018).
- 488 31. S. Civciristov, *et al.*, Preassembled GPCR signaling complexes mediate distinct cellular responses to ultralow  
489 ligand concentrations. *Sci. Signal.* **11**, eaan1188 (2018).
- 490 32. K. Qin, C. Dong, G. Wu, N. A. Lambert, Inactive-state preassembly of G(q)-coupled receptors and G(q)  
491 heterotrimers. *Nat. Chem. Biol.* **7**, 740–747 (2011).

492 33. C. Galés, *et al.*, Probing the activation-promoted structural rearrangements in preassembled receptor-G protein  
493 complexes. *Nat. Struct. Mol. Biol.* **13**, 778–786 (2006).

494 34. M. Nobles, A. Benians, A. Tinker, Heterotrimeric G proteins precouple with G protein-coupled receptors in  
495 living cells. *PNAS* **102**, 18706–18711 (2005).

496 35. W. M. Oldham, H. E. Hamm, Heterotrimeric G protein activation by G-protein-coupled receptors. *Nat. Rev.*  
497 *Mol. Cell Biol.* **9**, 60–71 (2008).

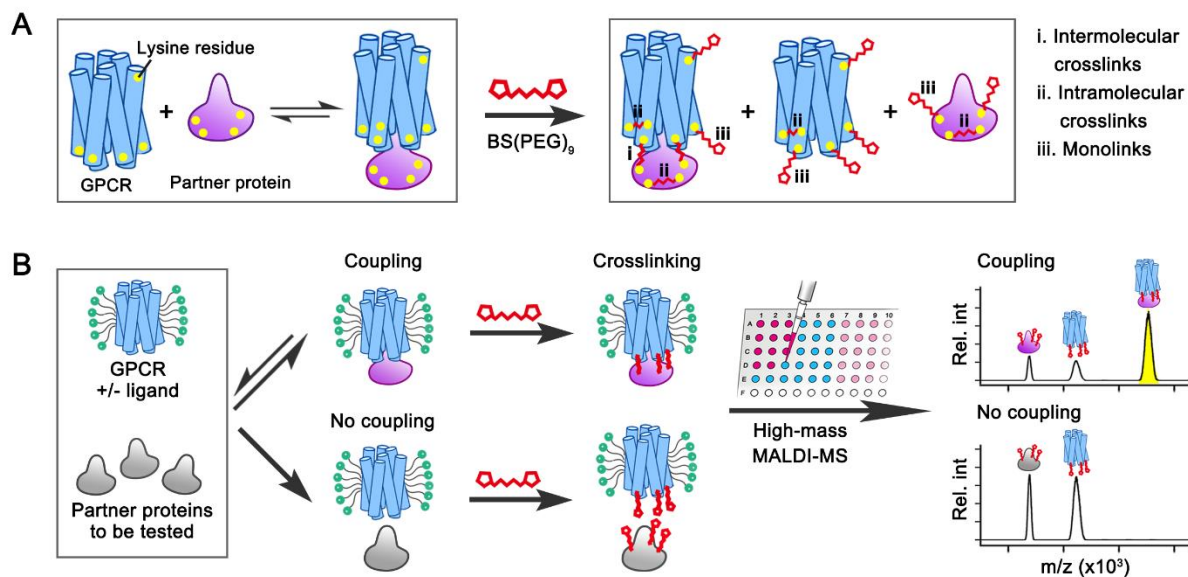
498 36. T. Flock, *et al.*, Selectivity determinants of GPCR–G-protein binding. *Nature* **545**, 317–322 (2017).

499 37. B. R. Conklin, Z. Farfel, K. D. Lustig, D. Julius, H. R. Bourne, Substitution of three amino acids switches  
500 receptor specificity of Gq alpha to that of Gi alpha. *Nature* **363**, 274–276 (1993).

501 38. T. Warne, P. C. Edwards, A. S. Doré, A. G. W. Leslie, C. G. Tate, Molecular basis for high-affinity agonist  
502 binding in GPCRs. *Science* **364**, 775–778 (2019).

503 39. N. P. Martin, E. J. Whalen, M. A. Zamah, K. L. Pierce, R. J. Lefkowitz, PKA-mediated phosphorylation of  
504 the beta1-adrenergic receptor promotes Gs/Gi switching. *Cell Signal* **16**, 1397–1403 (2004).

505  
506  
507  
508  
509  
510  
511  
512  
513  
514  
515  
516  
517  
518  
519



520

521 **Fig. 1.** Workflow for the analysis of the selective coupling between GPCRs and partner proteins via high-

522 mass MALDI-MS. (A) Schematic of the crosslinking procedure resulting in stabilised GPCR•G-protein

523 complex plus unbound partners “decorated” with monolinks. (B) For assessing the ligand-mediated

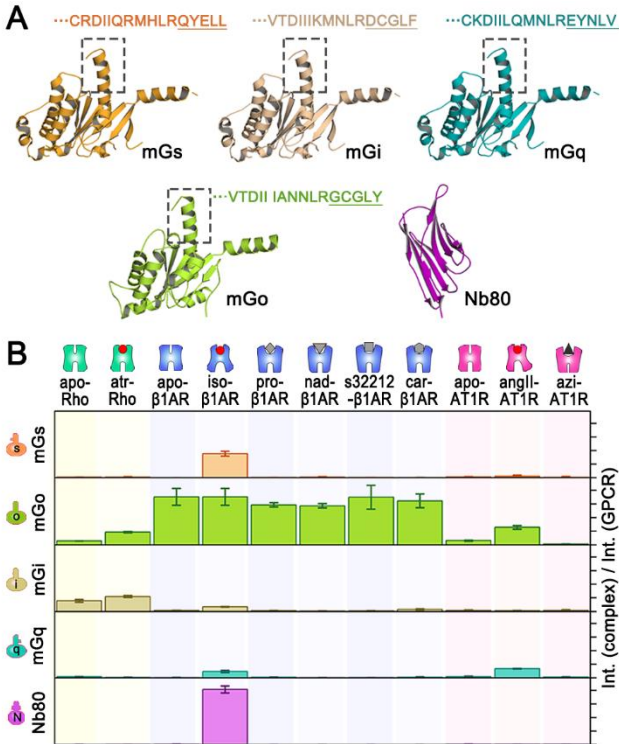
524 selectivity of a GPCR to a partner protein, the GPCR is first incubated with a mGα, nanobody 80 (Nb80),

525 or G-protein, in the presence or absence of ligand (*SI Appendix*, Table S3). The GPCR•partner complexes

526 formed are then stabilised by chemical crosslinking, followed by detection of the protein components by

527 high-mass MALDI-MS.

528

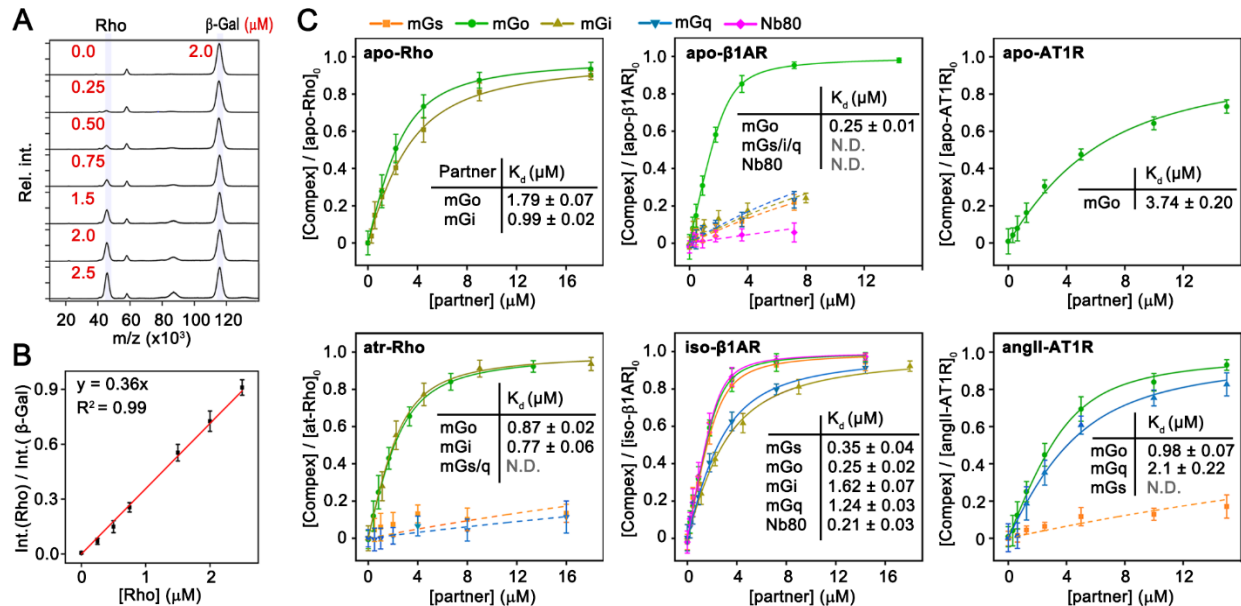


529

530 **Fig. 2.** Selectivity in complex formation of apo- and ligand-bound GPCRs with partner proteins assayed by  
 531 high-mass MALDI-MS. (A) Three-dimensional structural models of mGα proteins and Nb80. The amino  
 532 acid sequences of the C-terminal tail (helix 5, box) of the Gα subunit, accounting for ~70% of the interacting  
 533 surface between GPCRs and G proteins, are shown for all mGα proteins (homology models of mGi, and  
 534 mGq were built using SWISS-MODEL with mGs, PDB – 3SN6, as template); the last five key amino acids  
 535 in mGα involved in selectivity determinant are underlined. (B) Complex formation propensity of three  
 536 GPCRs – Rho, β1AR, and AT1R – in the presence or absence of agonists, antagonists, or inverse agonists  
 537 with their partner proteins mGs, mGo, mGi, mGq and Nb80 is measured by comparing the relative peak  
 538 intensity of the GPCR•partner protein complex with that of the non-complexed GPCR. The ligands used  
 539 were atr = all trans-retinal, iso = isoprenaline, pro = propranolol, nad = nadolol, car = carvedilol, angII =  
 540 angiotensin II, azi = azilsartan (*SI Appendix*, Table S3); apo designates the ligand-free forms. Error bars  
 541 represent standard deviations determined from three independent replicates.

542

543



544

545 **Fig. 3.** Binding affinities between GPCRs and partner proteins. (A) Calibration of different concentrations

546 of Rho normalized to 2  $\mu\text{M}$  of  $\beta$ -galactosidase. (B) Peak intensity ratio of Rho to  $\beta$ -galactosidase vs. Rho

547 concentration in the sample. (C) Evaluation of the affinities (dissociation constants  $K_d$ , measured in  $\mu\text{M}$ )

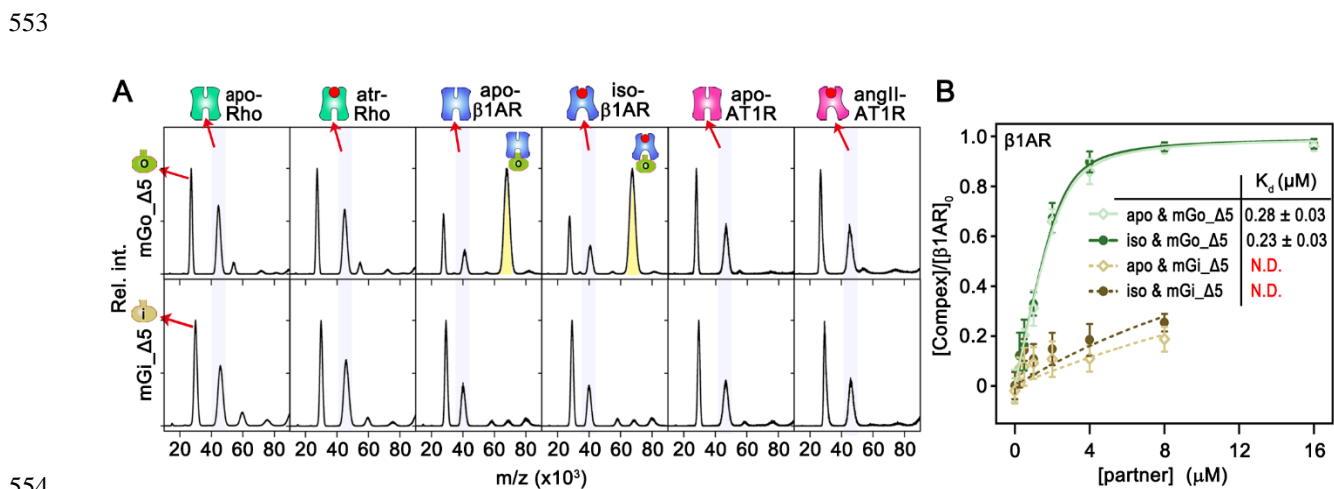
548 for different GPCR with various partner proteins (mGs – orange, mGo – green, mGi – beige, mGo –

549 turquoise, and Nb80 – magenta), using both apo (top panels) and ligand-bound (bottom panels) forms of

550 the GPCRs. The data were obtained by titrating the G-protein against the GPCR in 20 mM Hepes buffer,

551 pH 7.5, 40 mM NaCl, 0.01% lauryl maltose neopentyl glycol (LMNG). Error bars represent standard

552 deviations from three independent replicates. N.D. = not determined.

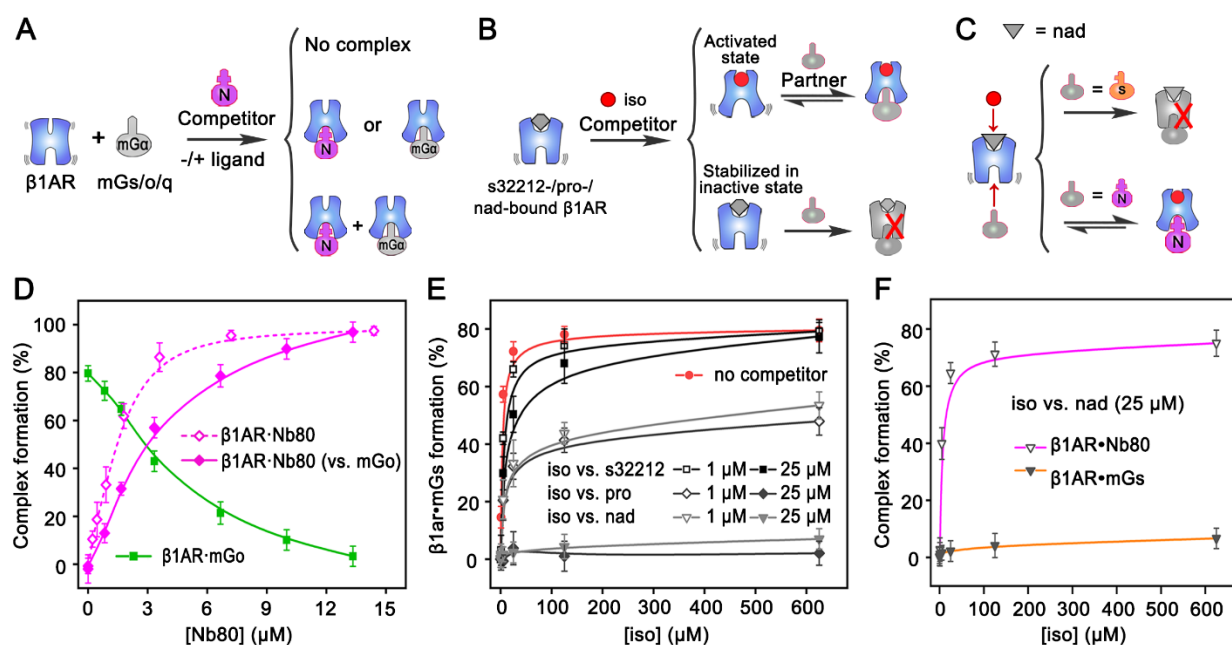


554



555 **Fig. 4.** Role of the C-terminus of mGo and mGi on binding to GPCRs. (A) Mass spectra showing the  
 556 coupling between ligand-bound GPCRs (from left to right: apo-Rho, atr-Rho, apo- $\beta$ 1AR, iso- $\beta$ 1A, apo-  
 557 AT1R, angII-AT1R) and truncated mGo (mGo\_Δ5, first row) and mGi (mGi\_Δ5, second row) proteins.  
 558 (B)  $K_d$  values of apo- $\beta$ 1AR•mGo\_Δ5, (solid light green empty squares), iso- $\beta$ 1AR•mGo\_Δ5 (dark green  
 559 solid circle), apo- $\beta$ 1AR•mGi\_Δ5 (light brown empty square), and iso- $\beta$ 1AR•mGi\_Δ5 (dark brown solid  
 560 square) (right panel). Error bars represent standard deviations from three independent repeats.

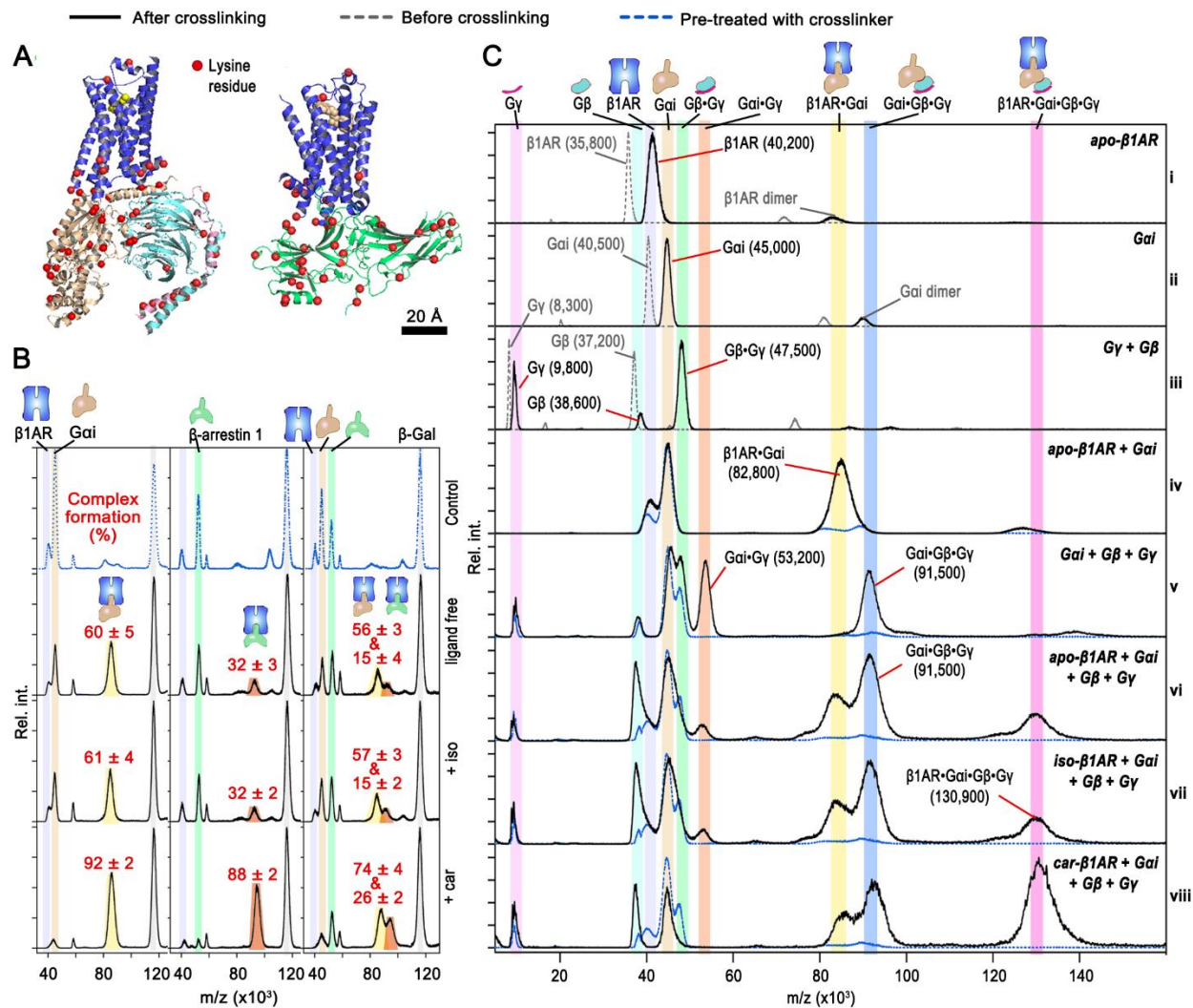
561



562

563 **Fig. 5.** Competition between partner proteins and between ligands for binding to GPCR. (A) Schematic of  
 564 the competition between Nb80 and other mG $\alpha$  proteins (mGs, mGo, and mGq) for binding to  $\beta$ 1AR (in the  
 565 presence or absence of ligand) and the different assembly possibilities. (B) Schematic of GPCR  
 566 conformational ensembles induced by the competition between antagonist and agonist ligands. The GPCRs  
 567 are stabilized in a suitable conformation under the combined effect of both ligands and partner proteins. (C)  
 568 Schematic of the competition between nadolol and isoprenaline and the formation of the  $\beta$ 1AR•Nb80  
 569 complex, modulated by the presence of a partner protein. (D) Conversion of  $\beta$ 1AR•mGo (solid green  
 570 circles) to  $\beta$ 1AR•Nb80 (solid magenta diamonds) using 2.5  $\mu$ M  $\beta$ 1AR, 3.0  $\mu$ M mGo, and increasing

571 concentrations of Nb80, and conversion to  $\beta 1AR \cdot Nb80$  in the absence of mGo (empty magenta diamonds).  
 572 (E)  $\beta 1AR \cdot mGs$  complex formation modulated by different ligands at different concentrations of  
 573 isoprenaline. (F) Comparison of the  $\beta 1AR \cdot mGs$  and  $\beta 1AR \cdot Nb80$  complex formation as revealed by  
 574 titration with isoprenaline. Error bars represent standard deviations from three independent repeats.  
 575



576  
 577 **Fig. 6.** Ligand-biased binding between  $\beta 1AR$  and  $G_i$ /arrestin proteins. (A) Structural models of the pentameric  
 578 complex  $\beta 1AR \cdot G\alpha_i \cdot G\beta \cdot G\gamma$  with bound isoprenaline (left; assembled using molecular graphics software  
 579 (PyMOL) and the templates 3SN6, 2Y03, and 1GP2), and  $\beta 1AR \cdot \beta$ -arrestin-1 complex (right; PDB code 6TKO)  
 580 with lysine residues highlighted in red. (B) Control experiment showing the absence of complex formation if  
 581 the interaction partners are first treated with crosslinker (top panel), and complex formation between  $\beta 1AR$  and

582  $G\alpha_i$ /arrestin/ $G\alpha_i$ +arrestin in ligand-free and isoprenaline- and carvedilol-bound receptor. Complex formation in  
583 percentages was calculated by normalisation with  $\beta$ -Gal as a standard. (C) Formation of diverse complexes of  
584  $G\alpha_i$ ,  $\beta$ ,  $G\gamma$ , and  $\beta$ 1AR following incubation and treatment with BS(PEG)<sub>9</sub>, in the absence and presence of  
585 isoprenaline or carvedilol. Grey dashed traces are spectra recorded without applying crosslinker, blue dashed  
586 traces are spectra recorded after pre-treating mixture components with crosslinker before incubation. Percentage  
587 complex formation are calculated from three independent repeats.